PCCP

PAPER

View Article Online
View Journal | View Issue

Cite this: *Phys. Chem. Chem. Phys.*, 2025, **27**, 13371

DFT and SISSO studies on the CO_2 cycloaddition reaction to ethylene oxide catalyzed by intraframework M(II)-BEA zeolites†

Winyoo Sangthong [a] and Jakkapan Sirijaraensre *[ab]

Received 8th April 2025,
Accepted 28th May 2025

DOI: 10.1039/d5cp01341k

rsc.li/pccp

CO_2 cycloaddition with EO over M(II)-intraframework BEA zeolites, with and without TMAI as a co-catalyst, is investigated using the M06-L functional. Without a co-catalyst, the catalytic process occurs through a concerted mechanism. The activation energy is calculated to be 39.9, 38.9, 38.6, and 39.6 kcal mol^{-1} for M-DeAlBEA zeolites (M = Ni, Cu, Zn, and Mg), respectively. In the presence of the co-catalyst, the catalytic process proceeds through three consecutive steps: ring opening, CO_2 activation, and ring closure, with the latter being the rate-determining step (RDS) of the reaction. The incorporation of TMAI plays a crucial role in activating EO and CO_2, leading to a more kinetically favorable formation of ethylene carbonate compared to the concerted pathway. From the energy span model, the activation energies of the RDS for the stepwise CO_2 cycloaddition are 16.8, 24.7, 14.7, and 14.1 kcal mol^{-1}, respectively. The SISSO algorithm has been employed to develop a mathematical expression for predicting the highest activation energy required for EC production *via* two pathways. The highest activation energy for CO_2 cycloaddition can be approximated using the molecular orbital (MO) energies of the zeolite and co-catalyst, along with the EO and CO_2 adsorption free energies. The SISSO-derived activation energies closely match the DFT-calculated values, achieving an R^2 value of 0.998 and an RMSE of 1.52 kcal mol^{-1}.

1. Introduction

Nowadays, the world is not just experiencing global warming; it is shifting towards a global boiling phenomenon that could have profound impacts on various areas, including agriculture, biodiversity, water resources, and human well-being.[1] The use of fossil fuels for energy generation and chemical production contributes significantly to environmental issues due to the rapid rise in greenhouse gases. Among these gases, carbon dioxide (CO_2) is critical in climate change due to its emission during energy production processes. Therefore, converting CO_2 into value-added chemical feedstocks is a promising approach to mitigating CO_2 emissions and reducing its environmental impact.[2–4] CO_2 is well-known as an abundant and non-toxic source of C1 building blocks. Therefore, several studies have focused on improving methods to convert CO_2 into higher-value chemicals using various processes including electrochemical reduction,[5,6] thermochemical conversion,[7,8] photocatalytic reduction,[9,10] catalytic CO_2 hydrogenation,[11,12] *etc.* One of the promising methods for converting a significant greenhouse gas into valuable chemicals is the cycloaddition of carbon dioxide to epoxides to form cyclic carbonates which are widely used in various applications, including polymerization reactions, battery technologies, pharmaceuticals, and as aprotic

[a] *Center for Advanced Studies in Nanotechnology for Chemical, Food, and Agricultural Industries, Kasetsart University Institute for Advanced Studies, Kasetsart University, Bangkok 10900, Thailand. E-mail: fscijkp@ku.ac.th*
[b] *Department of Chemistry, Faculty of Science, Kasetsart University, Bangkok 10900, Thailand*

† Electronic supplementary information (ESI) available: Table S1. Optimized geometrical parameters and NBO charges of the species involved in the CO_2 cycloaddition to EO over Ni-DeAlBEA in the presence of TMAI. Table S2. Optimized geometrical parameters and NBO charges of the species involved in the CO_2 cycloaddition to EO over Cu-DeAlBEA in the presence of TMAI. Table S3. Optimized geometrical parameters and NBO charges of the species involved in the CO_2 cycloaddition to EO over Zn-DeAlBEA in the presence of TMAI. Table S4. Optimized geometrical parameters and NBO charge of the species involved in the CO_2 cycloaddition to EO over Mg-DeAlBEA in the presence of TMAI. Table S5. Optimized geometrical parameters and NBO charges of the species involved in the adsorption of CO_2 over M-DeAlBEA (M = Ni, Cu, Zn and Mg). Table S6. Optimized geometrical parameters and NBO charges of the species involved in the concerted CO_2 cycloaddition to EO over M-DeAlBEA (M= Ni, Cu, Zn, and Mg). Table S7. Values of selected descriptors for the SISSO algorithms used to predict the activation free energy of the rate-determining step ($\Delta G^{\ddagger}$(RDS)). The E_{HOMO} and E_{LUMO} denote the highest occupied and the lowest unoccupied molecular orbital energies of the isolated zeolite, respectively. E_{HOMO}(TMAI) and E_{LUMO}(TMAI) represent the corresponding orbital energies of the isolated TMAI molecule. Fig. S1. Free energy profile for CO_2 cycloaddition with ethylene oxide and the optimized transition state geometry. Bond distances are given in Å. Fig. S2. Energetic profile for the ring-opening of EO by TMAI and optimized geometry of the transition state for the ring-opening of ethylene oxide by TMAI in the absence of a Lewis acid. Distances are given in Å. See DOI: **https://doi.org/10.1039/d5cp01341k**

polar solvents.[13–16] Thus, an efficient catalyst that can promote epoxide ring opening to produce an active intermediate for CO_2 cycloaddition is crucial for reducing energy consumption.

Generally, homogeneous catalysts have been widely used in the production of cyclic carbonates. Various types of homogenous catalysts have been used for this reaction such as quaternary ammonium salts,[17,18] metal complexes,[19,20] *etc.* Furthermore, the choline chloride-based deep eutectic solvent (DES) efficiently has been reported to be an efficient catalyst for the cycloaddition of propylene oxide (PO) with CO_2. The DES exhibits excellent catalytic performance in converting propylene oxide to cyclic carbonate with a 91% yield. The nucleophilicity of the halide ion plays a key role in the conversion of CO_2.[21,22] When the Cl^- anion was replaced with I^-, which has a higher nucleophilic ability, the ring-opening of the three-membered epoxide ring became significantly more favorable. As a result, the reaction proceeded more efficiently, allowing for a natural reduction at the required reaction temperature.[23] However, homogeneous catalysts exhibit certain limitations, such as the inability or difficulty in being separated from the reaction system for reuse and recycling. Furthermore, in some cases, their structures are significantly damaged under reaction conditions, compromising stability and reusability.[24]

The use of heterogeneous catalysts offers a promising solution for this conversion, as they overcome the limitations associated with homogeneous catalysts, such as challenges in scaling up for industrial applications and difficulties in catalyst recovery and separation from the products.[25–28] Previous studies have shown that heterogeneous catalysts, including metal oxides,[29,30] carbon-based materials,[31,32] metal–organic frameworks,[33–35] and zeolites,[36–38] can effectively promote the cycloaddition of CO_2 with epoxides to produce desired cyclic carbonates. Zeolites are crystalline materials with porous structures that serve as environmentally sustainable catalysts, facilitating chemical reactions while remaining in a separate phase from the products. In addition to metal-exchange zeolites that can catalyze the cycloaddition of CO_2 to epoxides, the incorporation of metal cations into the zeolite framework inspired by the formation of open Sn sites in the Sn-BEA zeolite[39] has received more attention. By introducing these metal cations into the zeolites, which have been pretreated with an acid to generate T-site vacancies, metal open sites are formed as Lewis acid sites. This modification not only enables fine-tuning of the acid–base characteristics of zeolites but also improves the stability of the active centers during chemical reactions.[40,41] Various types of metal cations have been added to the zeolite frameworks to act as active sites for chemical reactions. W. Liao and coworkers successfully synthesized isolated magnesium supported on a dealuminated BEA zeolite with the confined iodide ion inside the structure *via* the electrostatic interaction with tetraethylammonium cations. The catalyst was reported to exhibit extraordinary catalytic performance in the CO_2 cycloaddition to epoxides without the use of any solvent.[42] Besides Mg-supported dealuminated BEA, divalent metal cations such as Ni-, Cu-, and Zn-DeAlBEA zeolites were successfully synthesized.[43–46] These cations have been reported to be candidate active centers in homogeneous and heterogeneous systems for CO_2 cycloaddition.[47–50] However, the catalytic performance of these cations, in the form of zeolitic intraframework sites, in the conversion of CO_2 through cycloaddition with epoxides has not been reported.

According to previous studies,[51] divalent metal cations such as Cu, Ni, and Zn cations in the faujasite zeolite are active in catalyzing the epoxide cycloaddition with CO_2 without a co-catalyst. Cu-FAU is found to be more active than Ni- and Zn-FAU. Therefore, it is of interest to compare the effects of the location of these metal cations in the form of intraframework species with those of the extraframework species. Herein, we perform density functional theory (DFT) calculations to compare mechanistic and energetic details into the reaction mechanisms of CO_2 cycloaddition to epoxide over divalent Ni, Cu, Zn, and Mg supported on a dealuminated BEA zeolite in the absence and in the presence of tetraalkylammonium iodide which acts as an electrophilic agent. We compare the possible reaction mechanisms, energetic details, and the effect of metal on the catalytic reactivity. The calculated results would provide the fundamental knowledge for designing the zeolite-based catalytic systems for the CO_2 cycloaddition reaction. Additionally, we use the sure-independence screening and sparsifying operator (SISSO) method[52] to derive optimal mathematical models that describe the relationship between input features and outcomes. The resulting linear combinations of physical descriptors enable accurate prediction of target values. In this study, we apply the SISSO approach to estimate the activation energies of CO_2 cycloaddition using various DFT-derived descriptors related to electronic properties, such as atomic NBO charge, HOMO and LUMO energies, and adsorption energies. Based on the SISSO-based equation, this approach offers a computationally efficient method for screening the catalytic performance of related systems for this reaction before conducting time-intensive quantum chemical calculations to investigate the overall catalytic profile.

2. Models and methods

We employed density functional theory (DFT) calculations to investigate the possible reaction mechanisms of CO_2 cycloaddition of ethylene oxide (EO) catalyzed by divalent metal centers supported on dealuminated zeolite frameworks. The 38T cluster model, encompassing a nanometer-sized catalytic site that spans the intersection of two perpendicular 12-membered ring channels, was extracted from the crystal lattice of the BEA zeolite.[53] Previous studies have shown that this model is sufficiently large to determine the confinement effects of the zeolite framework.[54,55] To model a metal-supported DeAlBEA zeolite, an aluminum atom at the T9 position was removed and replaced with a divalent metal cation (Ni, Cu, Zn, or Mg) bound to two oxygen atoms within the channel. The remaining oxygen atoms were terminated with hydrogen atoms to form silanol groups. Previous studies have demonstrated that this position is the most stable for Zn grafted onto a dealuminated BEA zeolite.[56] As shown in Fig. 1, adsorbates and the zeolite's atoms

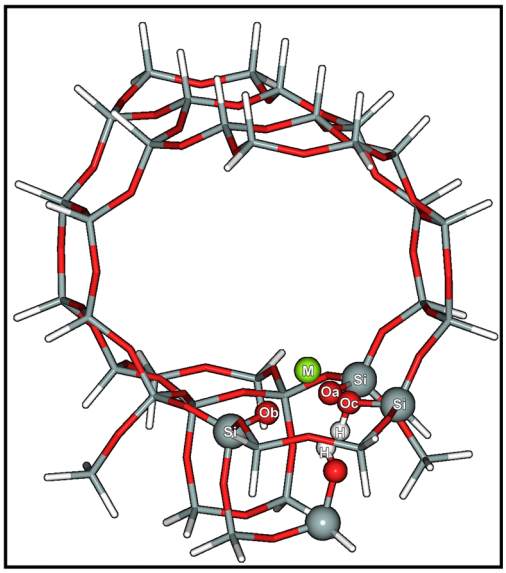

Fig. 1 Optimized structure of the M-DeAlBEA zeolites (M = Ni, Cu, Zn, and Mg).

around the substituted atom and terminal silanol groups were allowed to relax, while the remaining atoms were kept fixed at their crystallographic structures. *Ab initio* calculations based on density functional theory (DFT) were conducted using the M06-L functional, as implemented in the Gaussian 09 software package.[57] The M06 functionals, particularly M06-L,[58] have not only been highly effective in the confinement effects within zeolites but also effectively described the differences among zeolites with varying pore sizes and the stabilization of transition states in metal-zeolite systems.[59–61] A mixed basis set was employed for geometry optimization throughout the catalytic process. The LANL2DZ effective core potentials were used for transition metals and the iodine atom, while the 6-31G(d,p) basis set was applied for Mg and nonmetal atoms. The electronic ground state was set to triplet and doublet for Ni- and Cu-DeAlBEA zeolites, respectively, while the singlet state was used for Zn- and Mg-DeAlBEA systems. The spin states of all complexes along the reaction coordinate in these systems remained unchanged. In this study, tetramethylammonium iodide (TMAI) was chosen to represent the nucleophilic agent. Vibrational frequency analysis was conducted to confirm the transition state structures following geometric optimization. All reported energies are Gibbs free energies at 298.15 K and 1 atm. Additionally, natural bond orbital (NBO) analysis was carried out to determine charge distributions and orbital interactions within the complexes.[62]

3. Results and discussion

3.1. M-DeAlBEA zeolites (M = Ni, Cu, Zn, and Mg) and EO and CO_2 adsorption complexes

In this study, the 38T cluster representing divalent cation-supported DeAlBEA zeolite acts as a catalyst for the cycloaddition of CO_2 to ethylene oxide to form ethylene carbonate. The optimized structures and their electronic properties were evaluated by the M06-L level of theory. Selected optimized structures, important structural parameters of these adsorption complexes, and their NBO atomic charges of M-DeAlBEA (M = Ni, Cu, Zn, and Mg) systems are reported in Tables S1–S4 of the ESI.† For the optimized structure of the zeolite active site, it was found that the cation is sited over and compensated for by two oxygen atoms with shorter distances and has a small interaction with one silanol group around the dealuminated position. After deposition on the dealuminated site, partial electron transfer occurs from the zeolite framework to the divalent metal ions. The NBO charge of the cation is calculated to be +1.18*e*, +1.16*e*, +1.53*e*, and +1.67*e*, for M-DeAlBEA zeolites (M = Ni, Cu, Zn, and Mg), respectively.

Firstly, the adsorption complexes of EO on these catalysts, designated as ADS1, were investigated. The optimized structures of EO adsorbed on the M-DeAlBEA systems (M = Ni, Cu, Zn, and Mg) are shown in Fig. 2. Their selected optimized parameters and NBO charges are reported in Tables S1–S4 (ESI†), respectively. The interaction results from the oxygen atom of EO interacting with the Lewis acidic sites present in the M-DeAlBEA zeolites *via* its lone paired electrons. The intermolecular distances between the oxygen atom of EO and the metal cation in these systems range from 2.00 to 2.06 Å. When EO binds to the metal center of the system, the metal of the catalyst polarizes the C–O bond of the epoxide. This results in a more negatively charged O1 atom by about −0.1*e* in the adsorption complex. The adsorption of these systems has a slight effect on

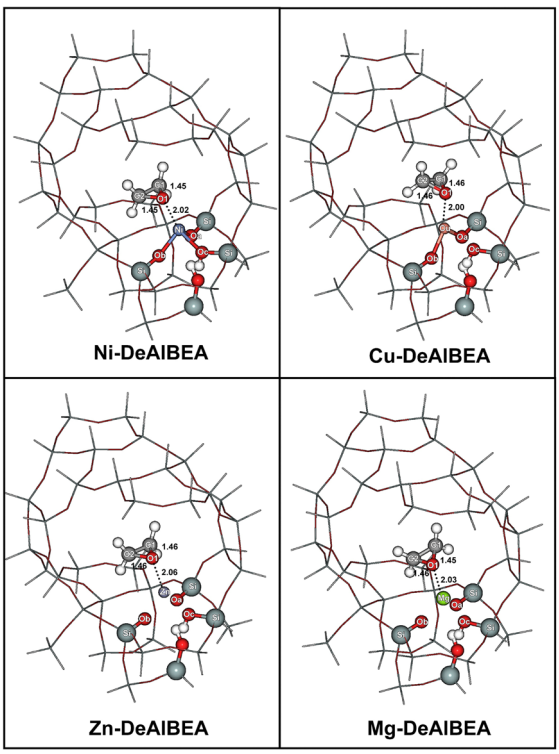

Fig. 2 Optimized structures of the ethylene oxide adsorption complexes on M-DeAlBEA zeolites (M = Ni, Cu, Zn, and Mg). Distances are in Å.

the EO molecule. Even though the adsorption free energy on these systems is in the range of chemisorption, which is greater than 20 kcal mol^{-1}, the deformation free energy of the EO molecule in all systems is only about 0.9 kcal mol^{-1}. Except for Cu-DeAlBEA, the adsorption free energy of the EO complex follows the trend of the metal cation charge. The higher the positive charge of the metal, the stronger the interaction between the EO molecule and the zeolite. The adsorption free energies are predicted to be −19.8, −24.5, and −26.0 kcal mol^{-1} for the Ni-, Zn-, and Mg-DeAlBEA zeolites, respectively. In the case of the Zn- and Mg-DeAlBEA zeolites, the amount of electron transfer is 0.08*e* and 0.06*e* for Zn- and Mg-DeAlBEA zeolites, which are less than that of the other systems (0.12*e* and 0.13*e*). This indicates that the interaction of an EO molecule on the active center is dominated by the electrostatic interaction. In the case of Cu-DeAlBEA, the atomic charge of Cu is less than that of the Ni-DeAlBEA zeolite. The adsorption free energy of the former system, which is slightly greater than that of the latter, is calculated to be −22.1 kcal mol^{-1}. Because the Lewis acidity of Cu-DeAlBEA is greater than that of Ni-DeAlBEA as indicated by the lower energy of the LUMO (−5.89 eV for Cu *vs.* −4.42 eV for Ni), there is a slight difference in the amount of electron transfer from the EO molecule to the zeolite. As a result, the energy of EO adsorption is slightly higher in Cu-DeAlBEA.

For CO_2 adsorption, selected geometric parameters and their NBO charges for the CO_2 adsorption complexes on the M-DeAlBEA zeolites (M = Ni, Cu, Zn, and Mg) are provided in Table S5 (ESI†). Their optimized structures are depicted in Fig. 3. The CO_2 molecule binds to the metal center of the dealuminated zeolite through its oxygen lone-pair electrons. The distances between the metal and the bounded oxygen atom are in the range of 2.11 to 2.19 Å. The linear structure of CO_2 is slightly bent upon the adsorption. The NBO analysis observed that CO_2 donates a small amount of electron density from the oxygen *p* orbital to the vacant orbitals of the metal. The bond angle of M–O3–C3 is predicted to be 146.3°, 137.6°, 136.9°, and 139.6° for the adsorption on M-DeAlBEA zeolites (M = Ni, Cu, Zn, and Mg), respectively. The net charge of the CO_2 molecule is slightly positive, with a value of 0.06*e* to 0.08*e*. The two C═O bonds of the adsorbed CO_2 become slightly asymmetrical, measuring 1.18 Å and 1.16 Å together with the bound oxygen charge decrease from −0.51*e* to −0.58*e*, −0.58*e*, −0.61*e*, and −0.62*e* for M-DeAlBEA zeolites (M = Ni, Cu, Zn, and Mg), respectively. The adsorption free energies are calculated to be −5.7, −5.0, −7.0, and −8.6 kcal mol^{-1}. It was also found that the interaction of the EO molecule with the metal centers of the DeAlBEA zeolite is approximately three to four times stronger than the interaction of CO_2. As a result, the presence of CO_2 in the catalytic system does not hinder the adsorption of EO on the metal center, which is a critical initial step in the CO_2 cycloaddition process.

3.2. The mechanism of CO_2 cycloaddition on the M-DeAlBEA zeolite (M = Ni, Cu, Zn, and Mg)

As previously mentioned, the Mg-DeAlBEA zeolite with confined iodide anions was successfully synthesized and demonstrated

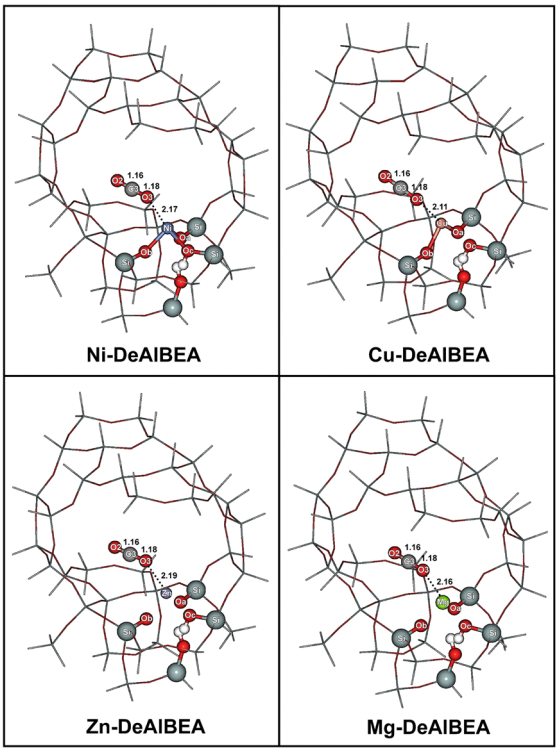

Fig. 3 Optimized structures of the carbon dioxide adsorption complexes on M-DeAlBEA zeolites (M = Ni, Cu, Zn, and Mg). Distances are in Å.

excellent performance in CO_2 cycloaddition to epoxides. Therefore, the catalytic mechanism of CO_2 cycloaddition of ethylene oxide to form ethylene carbonate over M-DeAlBEA zeolites (M = Ni, Cu, Zn, and Mg) in the presence of TMAI has been investigated. Without a catalyst, the activation free energy ($\Delta G^{\ddagger}$) for the conversion of CO_2 and ethylene oxide (EO) is predicted to be 62.1 kcal mol^{-1} (*cf.* Fig. S1, ESI†), indicating that this uncatalyzed reaction is kinetically unfavorable. Therefore, a catalyst is needed for this conversion. From previous studies, the catalytic cycloaddition is proposed to proceed through a stepwise mechanism,[63,64] as illustrated in Scheme 1. The CO_2 cycloaddition over the catalyst initiates the adsorption of ethylene oxide (EO) on the metal center and is envisioned to proceed through three elementary steps. First, the three-membered ring of ethylene oxide (EO) is opened by the iodide ion from TMAI, which acts as a nucleophile. It attacks the carbon of the adsorbed epoxide, leading to the formation of a surface alkoxide intermediate. Second, CO_2 is inserted into the surface alkoxide intermediate, forming a carbonate intermediate

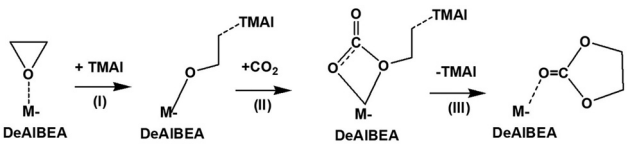

Scheme 1 Proposed catalytic process of CO_2 cycloaddition to ethylene oxide (EO) catalyzed by M-DeAlBEA zeolites (M = Ni, Cu, Zn, and Mg) in the presence of tetramethylammonium iodide (TMAI): (I) EO ring opening, (II) CO_2 insertion, and (III) ring closure.

at the metal sites. Third, the carbonate intermediate undergoes ring closure through a five-membered ring transition state, leading to the formation of a cyclic carbonate and the regeneration of the catalyst. The selected optimized structures and the corresponding NBO charges for the elementary steps of CO_2 cycloaddition to EO over M-DeAlBEA zeolites (M = Ni, Cu, Zn, and Mg) in the presence of TMAI are presented in Tables S1–S4 (ESI†), respectively.

The first step of the reaction starts with the co-adsorption of EO on the metal active site of the catalyst and TMAI inside the zeolite pore, designated as ADS2 (*cf.* Fig. 4a). From this complex, TMAI promotes the nucleophilic ring-opening of the epoxide by activating the C–O bond through nucleophilic attack by I^- (*cf.* Fig. 4b). In all systems, the C2–O1 bond distance is elongated from the adsorption complex by about 0.3 Å. The alkyl iodide has a bond distance of about 2.8 Å. The negative charge of the iodide is reduced from $-0.83e$ to about $-0.6e$ at the transition state (TS1), indicating the transfer of the electron from the iodide ion into the antibonding orbital of the C–O bond. The imaginary frequencies of $339.1i$ (Ni), $380.6i$ (Cu), $329.3i$ (Zn), and $306.8i$ cm^{-1} (Mg) are associated with the dissociation of the C2–O1 bond and the formation of the C2–I bond. These transition states in all systems have a relative energy lower than the adsorption of the EO adsorption complex (ADS1). This step has an activation energy of 5.6, 6.8, 4.0, and 2.9 kcal mol^{-1} for the catalysis on M-DeAlBEA zeolites (M = Ni, Cu, Zn, and Mg), respectively. The Lewis acid sites in M-DeAlBEA (M = Ni, Cu, Zn, Mg) zeolites play a key role in lowering the activation energy for the ring-opening step by stabilizing its transition state. Without the Lewis acid, the ring opening of ethylene oxide by only TMAI requires an activation energy of 32.4 kcal mol^{-1} (*cf.* Fig. S2 in the ESI†). This observation is in accordance with the theoretical study of CO_2 cycloaddition to propylene epoxide catalyzed by ammonium ferrates.[65]

After the first transition state, the metal–alkoxide intermediate (INT1) is formed (*cf.* Fig. 4c). In all systems, the formation of INT1 is an exothermic process relative to the isolated system of about -35 kcal mol^{-1}. The significantly greater stability of INT1 compared to the adsorption step indicates that its formation is an irreversible process. The M–O1 bond distance gradually decreases compared to the values observed in the adsorption (ADS1) and transition state (TS1) steps. Methylene carbon is bound to the iodide ion with a bond distance ranging from 2.24 to 2.27 Å. According to the NBO analysis, the calculated Wiberg bond order indices between the metal and the oxygen atom are 0.440 (Ni–O1), 0.466 (Cu–O1), 0.345 (Zn–O1), and 0.269 (Mg–O1). The atomic charges of the oxygen (O1) atom in INT1 become more negative than that of the isolated EO molecule, indicating an increase in the nucleophilicity of the O1 atom after the ring-opening process.

The next step is the activation of CO_2, which begins with the adsorption of CO_2 onto the metal–alkoxide oxygen atom (CO_2-INT1), as shown in Fig. 5a. The CO_2 carbon atom interacts with the oxygen atom of INT1. This step is a slightly endergonic process with a free energy of about 1 kcal mol^{-1}. The distance between C3 and O1 is calculated to be 2.63 Å for Ni-DeAlBEA, 2.73 Å for Cu-DeAlBEA, 2.59 Å for Zn-DeAlBEA, and 2.59 Å for Mg-DeAlBEA, respectively. The adsorption of CO_2 on the surface alkoxide intermediate leads to distortion of the CO_2

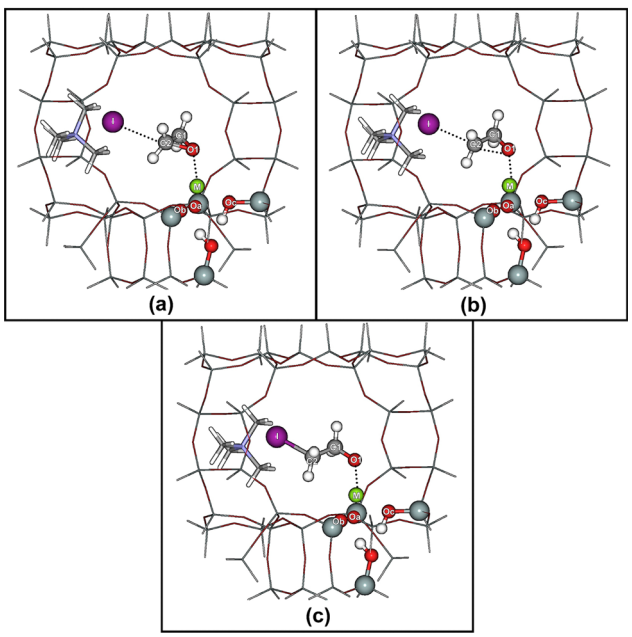

Fig. 4 Optimized structures of the EO ring-opening for the CO_2 cycloaddition to ethylene oxide over the M-DeAlBEA zeolites (M = Ni, Cu, Zn, and Mg): (a) EO–TMAI adsorption complex (ADS2), (b) transition state (TS1), and (c) metal–alkoxide intermediate (INT1).

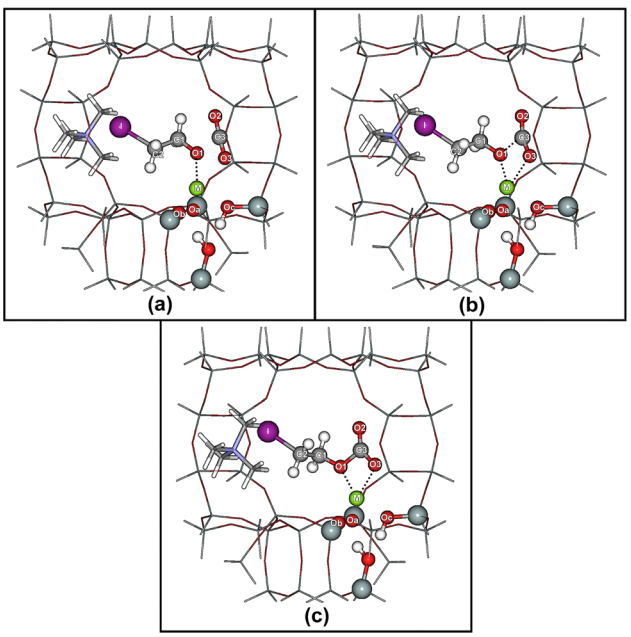

Fig. 5 Optimized structures of the CO_2 insertion step for the CO_2 cycloaddition to ethylene oxide over the M-DeAlBEA zeolites (M = Ni, Cu, Zn, and Mg): (a) coadsorption complex (CO_2-INT1), (b) the second transition state (TS2), and (c) carbonate intermediate (INT2).

structure, causing it to shift from a linear to a slightly bent configuration with a bond angle of about 176°. This leads to a slight imbalance in the NBO charge on the two oxygen atoms of CO_2. The activation of the CO_2 molecule takes place *via* the TS2 transition state, which involves the insertion of CO_2 in the alkoxide bond to produce a carbonate-like intermediate (INT2).

At the second transition state (*cf.* Fig. 5b), the CO_2 carbon atom attaches to O1 of INT1 with distances of 1.83 Å for Ni-DeAlBEA, 1.81 Å for Cu-DeAlBEA, 1.84 Å for Zn-DeAlBEA, and 1.92 Å for Mg-DeAlBEA, respectively. Simultaneously, the C–O bond distances of the attached CO_2 become more asymmetrically stretched, with the C3–O3 bond lengthening more than the C3–O2 bond. The bond between the metal and O1 is lengthened, while the distance between the metal and O3 becomes shorter. The imaginary frequency obtained from a normal mode analysis at 226.4*i* cm^{-1} (Ni-DeAlBEA), 240.6*i* cm^{-1} (Cu-DeAlBEA), 186.0*i* cm^{-1} (Zn-DeAlBEA), and 170.4*i* cm^{-1} (Mg-DeAlBEA) corresponds to the movement of CO_2 to form the C3–O1 bond. The activation energy for CO_2 insertion is 7.4 kcal mol^{-1} for Ni-DeAlBEA, 8.4 kcal mol^{-1} for Cu-DeAlBEA, 4.4 kcal mol^{-1} for Zn-DeAlBEA, and 3.2 kcal mol^{-1} for Mg-DeAlBEA. The activation energy height of this step corresponds to the strength of the alkoxide bond in INT1. Wiberg bond order indicates that the strength of the alkoxide bond between the oxygen atom (O2) of ethylene oxide and the metal center of the zeolites follows the order: Cu (0.466) > Ni (0.440) > Zn (0.345) > Mg (0.269). These values are in the range of the reported values in the related step on metal complexes. For instance, the activation free energy for the CO_2 insertion in the ring-opened PO intermediate on TM(II)-complexes with a Cl anion was reported to be 4.2 and 6.0 kcal mol^{-1} for Mg(II) and Zn(II), respectively.[66] A similar reaction has been reported for Zn(salphen) and Mg-porphyrin with I anion with values of 9.8 and 7.3 kcal mol^{-1}.[63,67] Additionally, a value of 4.8 kcal mol^{-1} was reported for the activation of CO_2 on the ring-opened epichlorohydrin/Zn(NCP)Cl complex with a TBAB co-catalyst.[68] These calculated results indicate that the deposition of the metal divalent cation into the framework of BEA zeolite still maintains the catalytic performance of these cations for the activation of the CO_2 molecule, as observed in homogeneous catalysts. After this step, the INT2 intermediate is formed. The relative free energy for the formation of INT2 is in the range of −25 to −35 kcal mol^{-1}. C3–O1 is covalently bonded with about 1.5 Å.

The ring closure of the INT2 is the final step of the CO_2 cycloaddition of EO, leading to the formation of ethylene carbonate (EC) (*cf.* Fig. 6a). Through an intramolecular cyclic S_N2-type reaction, the C2–O2 bond forms concurrently with the cleavage of the C2–I bond. In all systems, the C2–O2 distance is 2.00 Å, and the C2–I distance is about 2.7 Å. All transition states have only a single imaginary frequency with values of 328.2*i* cm^{-1} (Ni-DeAlBEA), 351.1*i* cm^{-1} (Cu-DeAlBEA), 327.6*i* cm^{-1} (Zn-DeAlBEA), and 323.2*i* cm^{-1} (Mg-DeAlBEA), respectively, corresponding to the formation of the C2–O2 bond and the cleavage of the C2–I bond. NBO analysis indicates that the back-donation of electrons from the Cu center to the deposited INT2 intermediate is greater than that to the intermediate on

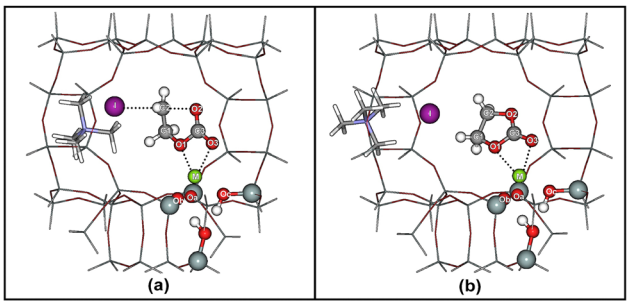

Fig. 6 Optimized structures of the ring closure step for the CO_2 cycloaddition to ethylene oxide over the M-DeAlBEA zeolites (M = Ni, Cu, Zn, and Mg): (a) the third transition state (TS3) and (b) product complex (PROD).

Ni, while the other systems do not exhibit this process. The NBO charge of the O2 atom is less negatively charged than that of others by about 0.03*e*. Therefore, the O2 atom in the case of Cu-DeAlBEA is less effective at interacting with the electrophilic carbon of the iodomethyl group, increasing the activation energy for the ring-closure step. The activation energy is calculated to be 10.2, 14.8, 12.0, and 12.7 kcal mol^{-1} for Ni-, Cu-, Zn-, and Mg-DeAlBEA zeolites, respectively. This step is found to be the rate-determining step in the CO_2 cycloaddition with ethylene oxide catalyzed by M-embedded BEA zeolites. The height of the energy barrier is directly proportional to the nucleophilicity of the O2 atom in the intermediate INT2. The atomic charge of the O2 atom in the INT2 intermediate on the Cu-DeAlBEA zeolite is less negative than in other systems. This is mainly due to the slightly stronger electron back-donation from Cu(II) to the INT2 intermediate compared to the other cations, which results in a weaker covalent bond between the C3 and O1 atoms. Consequently, electron redistribution to the C3–O2 bond occurs, making the C3–O2 bond slightly shorter and stronger in Cu-DeAlBEA than in the other systems. For metal complexes, the activation energy of this step CO_2/propylene oxide cycloaddition was reported in the range of 1.5 to 17.5 kcal mol^{-1} depending on the type of metal cation and the co-catalyst.[66,69–71] Among selected divalent cations, Cu-DeAlBEA is not the candidate for the CO_2 cycloaddition with ethylene oxide incorporated with the TMAI co-catalyst. After this process, the coadsorption of cyclic carbonate and the TMAI complex on the metal center of the catalyst has relative free energies of −33.7, −36.9, −37.0 and −38.8 kcal mol^{-1} for M-DeAlBEA (M = Ni, Cu, Zn, and Mg), respectively.

Fig. 7 demonstrates the energy profiles for the stepwise reaction mechanism of CO_2 cycloaddition to EO on Ni-, Zn-, Cu-, and Mg-DeAlBEA zeolites, respectively. With the presence of iodide anion that stabilized in the zeolite framework with the electrostatic interaction with tetramethylammonium cation, the cleavage of the epoxide C–O bond could be facilitated and activated by the incorporation of metal and iodide ion in the first step. The formation of the metal alkoxide intermediate is identified as an exergonic process. The subsequent step involves the insertion of CO_2 into the metal–alkoxide bond. The calculated activation energies for these two steps range from 3 to 8 kcal mol^{-1}. The ring-closure of the carbonate

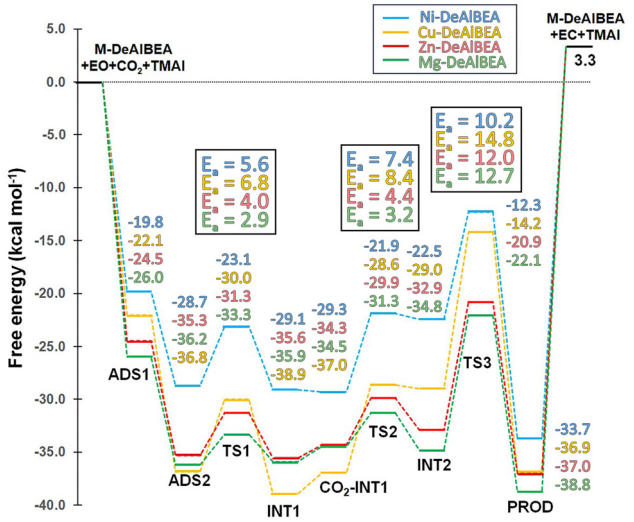

Fig. 7 Free energy profiles for the stepwise mechanism of the CO_2 cycloaddition to ethylene oxide over Ni-DeAlBEA (blue line), Cu-DeAlBEA (yellow line), Zn-DeAlBEA (red line), and Mg-DeAlBEA (green line) in the presence of TMAI.

intermediate is the rate-determining step, and the activation energies are in the order of Ni-DeAlBEA (10.2 kcal mol^{-1}) < Zn-DeAlBEA (12.0 kcal mol^{-1}) < Mg-DeAlBEA (12.7 kcal mol^{-1}) < Cu-DeAlBEA (14.8 kcal mol^{-1}).

According to the previous study,[51] these cations on the FAU zeolite can promote the conversion of CO_2 *via* cycloaddition with ethylene oxide. The catalytic trend is reported as follows: Cu(II)-FAU > Ni(II)-FAU ≈ Zn(II)-FAU. Therefore, it is of interest to study the catalytic performance of the M(II)-embedded BEA zeolites for this reaction without the co-catalyst (*cf.* Scheme 2). The optimized structures and important parameters of transition states and products for this mechanism are illustrated in Fig. 8 and 9 and the energy profiles for the cycloaddition of EO with CO_2 on M-DeAlBEA (M = Ni, Cu, Zn, and Mg) are shown in Fig. 10. Their selected geometrical parameters and NBO charges are documented in Table S6 (ESI†). At the transition state, CO_2 interacts with the ring-opened EO fragment. The C2–O1 bond of adsorbed EO is cleaved. Concurrently, two C–O bonds between the ring-opened EO and CO_2 become shortened with distances of approximately 1.9 and 2.5 Å for the C2–O2 and C3–O1 distances, respectively. The imaginary frequency of these transition states is 248.2*i*, 300.2*i*, 322.8*i*, and 333.0*i* cm^{-1}, according to the formation of two C–O bonds between the ring-opened EO and CO_2 molecule on the metal center of

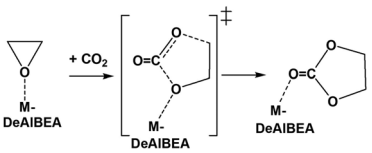

Scheme 2 Proposed concerted reaction mechanism for CO_2 cycloaddition of ethylene oxide (EO) over M-DeAlBEA zeolites (M = Ni, Cu, Zn, and Mg).

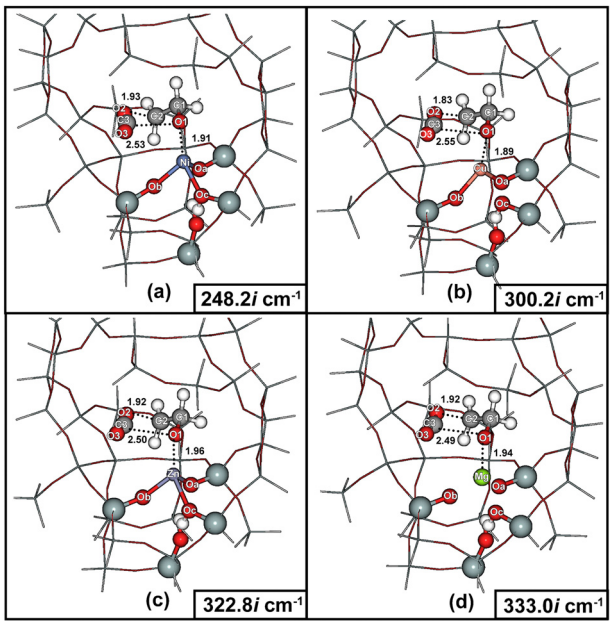

Fig. 8 Optimized structures of the transition state complex (TSc) for the concerted mechanism of the cycloaddition of EO with CO_2 over (a) Ni-DeAlBEA, (b) Cu-DeAlBEA, (c) Zn-DeAlBEA, and (d) Mg-DeAlBEA. Distances are in Å.

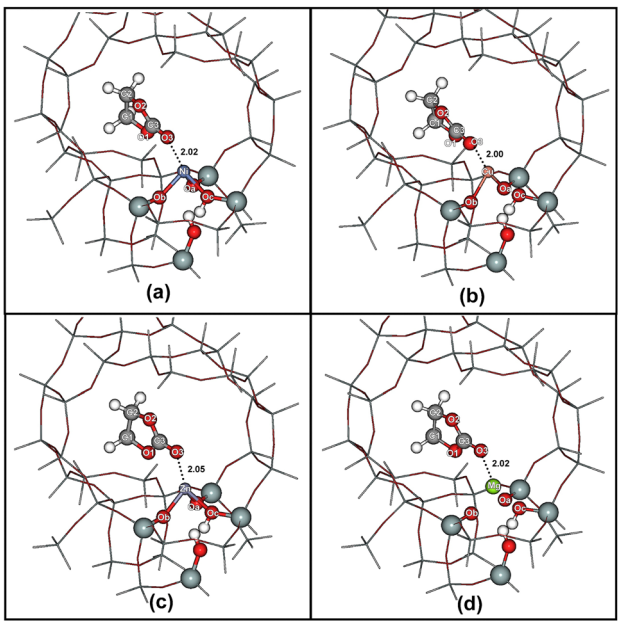

Fig. 9 Optimized structures of the EC adsorption complex (PRODc) for the concerted mechanism of the cycloaddition of EO with CO_2 over (a) Ni-DeAlBEA, (b) Cu-DeAlBEA, (c) Zn-DeAlBEA, and (d) Mg-DeAlBEA. Distances are in Å.

the M-DeAlBEA systems. The reaction has an activation barrier of 39.9, 38.9, 38.6, and 39.6 kcal mol^{-1} for CO_2 cycloaddition on Ni-, Cu-, Zn-, and Mg-DeAlBEA zeolites, respectively. Compared to the corresponding divalent cations in the FAU zeolite, Ni(II)- and Zn(II)-DeAlBEA show slightly higher activity, while Cu(II)-DeAlBEA exhibits slightly lower activity. It was found that the

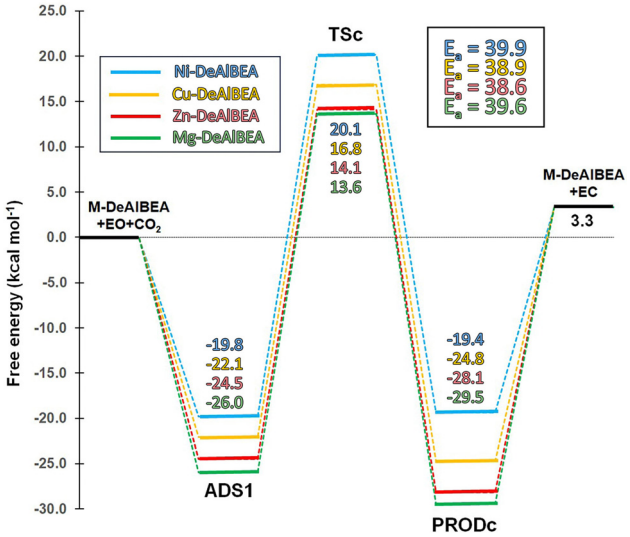

Fig. 10 Free energy profiles for the concerted mechanism of the CO_2 cycloaddition to ethylene oxide over Ni-DeAlBEA (blue line), Cu-DeAlBEA (yellow line), Zn-DeAlBEA (red line), and Mg-DeAlBEA (green line).

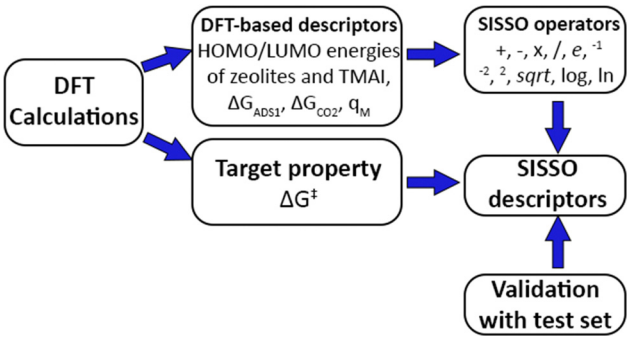

Fig. 11 Illustration of the workflow for fitting the predictive equation using the SISSO method.

back-donation from Cu to the deposited EO molecule is affected by the appearance of electron-donating groups from the zeolite frameworks. NBO analysis reveals that the net charge of EO at the transition state becomes less positive than the adsorption complex. The net charge is changed from +0.13*e* to +0.08*e*. This phenomenon is opposite to the observation in the Cu-FAU zeolite.[51]

Based on the optimized structures, the net NBO charge of the EO fragment is changed from +0.13*e* (ADS1) to +0.20*e* (TSc) for the CO_2 cycloaddition on the Cu(II)-FAU zeolite. The less positive charge indicates the more electrons on the deposited EO. Strong electron donation takes place *via* the donation of electrons from the paired-electron orbitals of the silanolates and the hydroxyl group from the dealuminated BEA zeolite to the unoccupied orbital of the Cu cation, resulting in the redistribution of the electrons in the deposited EO fragment *via* the back-donation process at the transition state. As a result, the catalytic performance of Cu(II) deposited in the BEA framework becomes less active than the exchanged Cu(II) on the FAU zeolite. The calculated results reveal the important effect of the zeolitic environment on the electronic properties of the Cu(II) cation for this reaction. Based on the activation energy of the concerted process, these M-embedded BEA zeolites do not catalytically promote the CO_2 cycloaddition with ethylene oxide without a co-catalyst.

The sure independence screening and sparsifying operation (SISSO) has been employed to find an efficient descriptor for generating the prediction model. We employ this method to identify descriptors for predicting the activation barriers of CO_2 cycloaddition with ethylene oxide, aiming to eliminate the need for time-intensive computational calculations. The SISSO method workflow for this study is shown in Fig. 11. The targeted result from the prediction model is the activation energy of the rate-determining step of the conversion of CO_2 *via* the cycloaddition reaction. Based on the energetic span model,[72] the rate-determining step of the reaction along the stepwise process on systems is the energy difference between the TOF-determining intermediate (TDI) and the TOF-determining transition state (TDTS). As shown in Fig. 7, the TDI is found to be the INT1 in the Ni-, Cu-, and Zn-De-AlBEA systems and the ADS2 in Mg-De-AlBEA. The TDTS state in all systems is the TS3 transition state. The difference in the energy of these two steps is called the apparent activation energy (δE). The δE values are calculated to be 16.8, 24.7, 14.7, and 14.1 kcal mol^{-1} for the catalytic process on M-DeAlBEA zeolites (M = Ni, Cu, Zn, and Mg) through the stepwise pathway. The electronic properties of the M(II) center on the dealuminated BEA zeolite and FAU zeolite[51] such as atomic NBO charge, HOMO and LUMO energies, and the adsorption energy of ethylene oxide, and CO_2 on the metal center have been used for creating the prediction model. For the M(II)-FAU zeolite, the NBO population analysis based on optimized structures was performed to calculate the electronic properties as in the M-De-AlBEA zeolite. To evaluate the reliability of the prediction model, parameters derived from Zn-DeAlBEA and Zn-FAU zeolites were employed as the test set parameters. Because the Zn(II) ion in these systems exhibit intermediate activity between the least and most effective cations. For the rate-determining step of the reaction, it was found that the activation energy of the catalytic process is proportional to two terms as shown in eqn (1).

$$\Delta G^{\ddagger} = 30.7[\exp(\Delta G_{\mathrm{ADS1}}) + \exp(E_{\mathrm{HOMO}}(\mathrm{TMAI}))] + 0.56\left[\left(\Delta G_{\mathrm{CO_2}} - \Delta G_{\mathrm{ADS1}}\right) + \left(E_{\mathrm{LUMO}} \times E_{\mathrm{HOMO}}(\mathrm{TMAI})\right)\right] \quad (1)$$

The first and second terms describe the role of the catalyst and the nucleophilicity of the co-catalyst in the activation free energy for the CO_2 cycloaddition reaction. In the absence of the co-catalyst, the activation free energy for the concerted CO_2 cycloaddition is governed by the second term. This term reflects the metal cation's acidity, which dictates its interactions with both EO and CO_2. Stronger coordination of EO to the metal center stabilizes the epoxide–metal intermediate, thereby increasing the energy barrier for CO_2 insertion into the epoxide ring. The sum of these two terms leads to the prediction of the

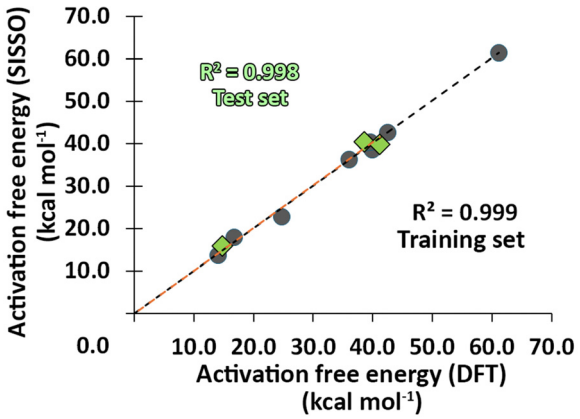

Fig. 12 Correlation between DFT-calculated and SISSO-predicted activation free energies for the rate-determining step on metal-zeolites. Circle symbols represent the training set, while diamond symbols represent the test set.

rate-determining step of the reaction for the formation of cyclic carbonate on the Lewis acid site of M(II)-zeolites. Their predicted activation energies and selected descriptors for SISSO algorithms in this work are documented in Table S7 (ESI†). A comparison between the predicted values from SISSO descriptors and the DFT values is shown in Fig. 12. A low RMSE (1.04 kcal mol^{-1}) and high R^2 value (0.999) between the results from DFT calculations and the SISSO prediction for the Ni-, Cu-, Mg-DeAlBEA and Cu-, and Ni-FAU zeolites indicate reliable results for using this equation for the prediction of catalytic performance of metal-zeolites in the CO_2 cycloaddition with and without a co-catalyst. For Zn-DeAlBEA, the SISSO-derived expression predicts apparent activation free energies of 16.0 kcal mol^{-1} (stepwise) and 40.5 kcal mol^{-1} (concerted), while for Zn–FAU (concerted) it predicts 39.9 kcal mol^{-1}. The DFT calculation is predicted to be 14.7, 38.6, and 41.2 kcal mol^{-1}. As shown in Fig. 12, an R^2 value of 0.998 indicates a consistent trend between the exact and predicted values from the SISSO method. An RMSE of 1.52 kcal mol^{-1} between the DFT values and all predicted SISSO values demonstrates the reliability of the activation energy obtained from the SISSO prediction. Compared to the computational demands for finding the TS structures along the catalytic process, the SISSO prediction based on the isolated complex and the EO and CO_2 adsorption complexes offers a viable way of screening potential catalysts for this reaction on zeolitic systems.

4. Conclusion

M06-L calculations are employed to investigate the CO_2 cycloaddition of ethylene oxide to form ethylene carbonate over an M(II)-intraframework dealuminated BEA zeolite (M-DeAlBEA). The catalytic processes are proposed to occur differently depending on the presence of the co-catalyst. Without a co-catalyst, the conversion of CO_2 and EO molecules takes place in a single step of the reaction without the formation of an intermediate. An activation free energy of about 40 kcal mol^{-1} for all systems indicates the inertness of these catalysts for the direct conversion of these molecules. In the presence of a co-catalyst, TMAI plays a crucial role in the activation of EO, leading to the formation of a ring-opened epoxide intermediate (INT1). INT1 is an active intermediate that can activate CO_2 facilely. These two steps occur sequentially and are kinetically favorable in all systems. The activation energies of these two steps are in the range of 3–8 kcal mol^{-1}. The last step, ring closure, is the rate-determining step of the reaction. Among selected catalysts, Cu-DeAlBEA is found to be the least active catalyst. The activation energy of this step is predicted to be 10.2, 14.8, 12.0, and 12.7 kcal mol^{-1} for Ni-, Cu-, Zn- and Mg-DeAlBEA zeolites, respectively. The stronger back-donation of Cu(II), compared to other systems, reduces the nucleophilicity of the terminal oxygen in the carbonate functional group, which plays a crucial role in ring closure to form the carbonate product. To facilitate the screening of potential catalysts for this reaction, the SISSO algorithm can provide a cost-effective tool for predicting the highest activation energy for the conversion of EO and CO_2 molecules with and without the co-catalyst by using descriptors. Four dominant descriptors as the LUMO energy of the zeolite, the HOMO energy of the co-catalyst, and the EO and CO_2 adsorption free energies are used as inputs to approximate the expected activation energy in the conversion of CO_2 and EO to the EC product. With respect to the DFT-based values, all predicted values of the highest activation free energy of the rate-determining step for the formation of cyclic carbonate are reasonably accurate, with a very small RMSE of 1.52 kcal mol^{-1}. The findings from this study offer valuable insights for designing efficient catalytic processes for CO_2 utilization.

Author contributions

Winyoo Sangthong: conceptualization, investigation, methodology, visualization, formal analysis, writing – original draft, and resources. Jakkapan Sirijaraensre: methodology, visualization, formal analysis, investigation, writing – review & editing, resources, and supervision.

Data availability

The data supporting this article have been included as part of the ESI.†

Conflicts of interest

There are no conflicts to declare.

Acknowledgements

This work was supported in part by grants from the Kasetsart University Research and Development Institute (KURDI), the Kasetsart University Institute for Advanced Studies (KUIAS) at Kasetsart University. The authors acknowledge the Department of Chemistry and the Kasetsart University Institute for Advanced Studies (KUIAS) for providing computing resources

that have contributed to the research results reported in this paper.

References

1 T. Amnuaylojaroen, *Adv. Meteorol.*, 2023, 580606.
2 L. Fu, Z. Ren, W. Si, Q. Ma, W. Huang, K. Liao, Z. Huang, Y. Wang, J. Li and P. Xu, *J. CO2 Util.*, 2022, **66**, 102260.
3 Y. Li, S. H. Chan and Q. Sun, *Nanoscale*, 2015, **7**, 8663–8683.
4 G. Fiorani, W. Guo and A. W. Kleij, *Green Chem.*, 2015, **17**, 1375–1389.
5 Q. Lu and F. Jiao, *Nano Energy*, 2016, **29**, 439–456.
6 S. Min Allah, A. H. Al-Marzouqi and F. M. Hassan, *Mater. Today Sustainability*, 2024, **27**, 100817.
7 X. Liu, H. Zhang, J. Du and J. Liao, *Process Saf. Environ. Prot.*, 2024, **189**, 1071–1086.
8 C. Graves, S. D. Ebbesen, M. Mogensen and K. S. Lackner, *Renewable Sustainable Energy Rev.*, 2011, **15**, 1–23.
9 P. Chen, Y. Zhang, Y. Zhou and F. Dong, *Nano Mater. Sci.*, 2021, **3**, 344–367.
10 D. Li, M. Kassymova, X. Cai, S. Q. Zang and H. L. Jiang, *Coord. Chem. Rev.*, 2020, **412**, 213262.
11 C. G. Okoye-Chine, C. O. L. Mbuya, N. C. Shiba and K. O. Otun, *Carbon Capture Sci. Technol.*, 2024, **13**, 100251.
12 C. Liu and Z. Liu, *Catalysts*, 2022, **12**, 1375.
13 N. Yadav, F. Seidi, D. Crespy and V. D'Elia, *ChemSusChem*, 2019, **12**, 724–754.
14 A. J. Kamphuis, F. Picchioni and P. P. Pescarmona, *Green Chem.*, 2019, **21**, 406–448.
15 E. J. C. Lopes, A. P. C. Ribeiro and L. M. D. R. S. Martins, *Catalysts*, 2020, **10**(5), 479.
16 B. B. Lu, J. Yang, Y. Y. Liu and J. F. Ma, *Inorg. Chem.*, 2017, **56**, 11710–11720.
17 V. Aomchad, S. Del Gobbo, P. Yingcharoen, A. Poater and V. D'Elia, *Catal. Today*, 2021, **375**, 324–334.
18 J. Li, C. Yue, W. Ji, B. Feng, M. Y. Wang and X. Ma, *Front. Chem. Sci. Eng.*, 2023, **17**, 1879–1894.
19 V. D'Elia and A. W. Kleij, *Green Chem. Eng.*, 2022, **3**, 210–227.
20 U. Bayer and R. Anwander, *Dalton Trans.*, 2020, **49**, 17472–17493.
21 K. Wu, T. Su, D. Hao, W. Liao, Y. Zhao, W. Ren, C. Deng and H. Lü, *Chem. Commun.*, 2018, **54**, 9579–9582.
22 M. Vagnoni, C. Samorì and P. Galletti, *J. CO2 Util.*, 2020, **42**, 101302.
23 F. Liu, Y. Gu, P. Zhao, H. Xin, J. Gao and M. Liu, *J. CO2 Util.*, 2019, **33**, 419–426.
24 D. J. Cole-Hamilton, *Science*, 2003, **299**, 1702–1706.
25 M. Alves, B. Grignard, R. Mereau, C. Jerome, T. Tassaing and C. Detrembleur, *Catal. Sci. Technol.*, 2017, **7**, 2651–2684.
26 X. Zhou, X. Yang, J. Yao and G. Wang, *Acta Chim. Sin.*, 2010, **68**, 870–874.
27 N. Kihara, N. Hara and T. Endo, *J. Org. Chem.*, 1993, **58**, 6198–6202.
28 Y. Zou, Q. Amuti, Z. Zou, Y. Xu, C. Yan, G. Cheng and H. Ke, *J. Colloid Interface Sci.*, 2024, **656**, 47–57.
29 J. Liu, B. Zhang, P. Jian and J. Shi, *Inorg. Chem.*, 2024, **63**, 12981–12991.
30 Y. Wei, Y. Li, Y. Xu, Y. Sun, T. Xu, H. Liang and J. Bai, *Front. Chem. Sci. Eng.*, 2024, **18**(5), 53.
31 C. Wang, Q. Song, K. Zhang, P. Liu, J. Wang, J. Wang, H. Zhang and J. Wang, *Chem. Commun.*, 2019, **55**, 1299–1302.
32 R. A. Molla, A. Iqubal, K. Ghosh and M. Islam, *ChemistrySelect*, 2016, **1**, 3100–3107.
33 P. Z. Li, X. J. Wang, J. Liu, H. S. Phang, Y. Li and Y. Zhao, *Chem. Mater.*, 2017, **29**, 9256–9261.
34 B. Parmar, P. Patel, R. S. Pillai, R. K. Tak, R. I. Kureshy, N. U. H. Khan and E. Suresh, *Inorg. Chem.*, 2019, **58**, 10084–10096.
35 P. Z. Li, X. J. Wang, J. Liu, J. S. Lim, R. Zou and Y. Zhao, *J. Am. Chem. Soc.*, 2016, **138**, 2142–2145.
36 D. Liu, G. Li, J. Liu, Y. Wei and H. Guo, *ACS Appl. Mater. Interfaces*, 2018, **10**, 22119–22129.
37 W. Liu, T. Xu, C. Li and J. Bai, *Inorg. Nano-Met. Chem.*, 2020, **50**, 1087–1093.
38 N. Nokhodiyan Isfahani, M. Bahadori, A. Marandi, S. Tangestaninejad, M. Moghadam, V. Mirkhani, M. Beheshti and N. Afzali, *Ind. Eng. Chem. Res.*, 2020, **59**, 11970–11978.
39 M. Boronat, P. Concepción, A. Corma, M. Renz and S. Valencia, *J. Catal.*, 2005, **234**, 111–118.
40 J. Zhang, L. Wang, G. Wang, F. Chen, J. Zhu, C. Wang, C. Bian, S. Pan and F. S. Xiao, *ACS Sustainable Chem. Eng.*, 2017, **5**, 3123–3131.
41 Y. Wan, M. Zhuang, S. Chen, W. Hu, J. Sun, J. Lin, S. Wan and Y. Wang, *ACS Catal.*, 2017, **7**, 6038–6047.
42 W. Liao, H. Lin, M. Yin, J. Zhang, Z. Zhu and H. Lü, *Fuel*, 2022, **323**, 124389.
43 X. Zhou, S. Wu, Y. Luo, L. Zhu and D. He, *Energy Fuels*, 2023, **37**, 450–458.
44 J. Janas, J. Gurgul, R. P. Socha and S. Dzwigaj, *Appl. Catal., B*, 2009, **91**, 217–224.
45 S. Dzwigaj, J. Janas, J. Mizera, J. Gurgul, R. P. Socha and M. Che, *Catal. Lett.*, 2008, **126**, 36–42.
46 L. Qi, Y. Zhang, M. A. Conrad, C. K. Russell, J. Miller and A. T. Bell, *J. Am. Chem. Soc.*, 2020, **142**, 14674–14687.
47 D. Rani, R. Kumar, V. Kumar and M. Singh, *Mater. Today Sustainability*, 2019, **5**, 100021.
48 S. C. Sau, P. K. Hota, S. K. Mandal, M. Soleilhavoup and G. Bertrand, *Chem. Soc. Rev.*, 2020, **49**, 1233–1252.
49 J. Tapiador, E. García-Rojas, P. López-Patón, G. Calleja, G. Orcajo, C. Martos and P. Leo, *J. Environ. Chem. Eng.*, 2023, **11**(2), 109497.
50 L. Xu, Y. Wang, Z. Sun, Z. Chen, G. Zhao, F. E. Kühn, W. G. Jia, R. Yun and R. Zhong, *Inorg. Chem.*, 2024, **63**, 1828–1839.
51 W. Sangthong and J. Sirijaraensre, *J. Mol. Graphics Modell.*, 2022, **117**, 108321.
52 R. Ouyang, S. Curtarolo, E. Ahmetcik, M. Scheffler and L. M. Ghiringhelli, *Phys. Rev. Mater.*, 2018, **2**, 083802.
53 J. B. Higgins, R. B. LaPierre, J. L. Schlenker, A. C. Rohrman, J. D. Wood, G. T. Kerr and W. J. Rohrbaugh, *Zeolites*, 1988, **8**, 446–452.

54 J. Sittiwong, K. Hiruntrakool, A. Rasrichai, O. Opasmongkolchai, P. Srifa, K. Nilwanna, T. Maihom, M. Probst and J. Limtrakul, *Microporous Mesoporous Mater.*, 2022, **341**, 112083.
55 W. Sangthong and J. Sirijaraensre, *New J. Chem.*, 2023, **47**, 12191–12199.
56 W. Jeevapong, J. Sittiwong, M. Probst, B. Boekfa, C. Wattanakit, T. Maihom and J. Limtrakul, *J. Phys. Chem. C*, 2023, **127**, 8473–8481.
57 M. J. Frisch, G. W. Trucks, H. B. Schlegel, G. E. Scuseria, M. A. Robb, J. R. Cheeseman,G. Scalmani, V. Barone, B. Mennucci, G. A. Petersson, H. Nakatsuji, M. Caricato, X. Li, H. P. Hratchian, A. F. Izmaylov, J. Bloino, G. Zheng, J. L. Sonnenberg, M. Hada, M. Ehara, K. Toyota, R. Fukuda, J. Hasegawa, M. Ishida, T. Nakajima, Y. Honda, O. Kitao, H. Nakai, T. Vreven, J. A. Montgomery Jr., J. E. Peralta, F. Ogliaro, M. J. Bearpark, J. Heyd, E. N. Brothers, K. N. Kudin, V. N. Staroverov, R. Kobayashi, J. Normand, K. Raghavachari, A. P. Rendell, J. C. Burant, S. S. Iyengar, J. Tomasi, M. Cossi, N. Rega, N. J. Millam, M. Klene, J. E. Knox, J. B. Cross, V. Bakken, C. Adamo, J. Jaramillo, R. Gomperts, R. E. Stratmann, O. Yazyev, A. J. Austin, R. Cammi, C. Pomelli, J. W. Ochterski, R. L. Martin, K. Morokuma, V. G. Zakrzewski, G. A. Voth, P. Salvador, J. J. Dannenberg, S. Dapprich, A. D. Daniels, Ö. Farkas, J. B. Foresman, J. V. Ortiz, J. Cioslowski and D. J. Fox, *Gaussian*, Gaussian Inc., Wallingford, CT, USA, 2009.
58 Y. Zhao and D. G. Truhlar, *Theor. Chem. Acc.*, 2008, **120**, 215–241.
59 T. Maihom, P. Khongpracha, J. Sirijaraensre and J. Limtrakul, *ChemPhysChem*, 2013, **14**, 101–107.
60 V. Paluka, T. Maihom, C. Warakulwit, P. Srifa, B. Boekfa, P. Treesukol, P. Poolmee and J. Limtrakul, *Chem. Phys. Lett.*, 2020, **754**, 137743.
61 S. Wannakao, C. Warakulwit, K. Kongpatpanich, M. Probst and J. Limtrakul, *ACS Catal.*, 2012, **2**, 986–992.
62 A. E. Reed, L. A. Curtiss and F. Weinhold, *Chem. Rev.*, 1988, **88**, 899–926.
63 F. Castro-Gómez, G. Salassa, A. W. Kleij and C. Bo, *Chem. - Eur. J.*, 2013, **19**, 6289–6298.
64 J. Sirijaraensre, *New J. Chem.*, 2019, **43**, 11692–11700.
65 N. Panza, R. Soave, F. Cargnoni, M. I. Trioni and A. Caselli, *J. CO2 Util.*, 2022, **62**, 102262.
66 P. Li and Z. Cao, *Organometallics*, 2018, **37**, 406–414.
67 Q. Wang, C. H. Guo, J. Jia and H. S. Wu, *J. Mol. Model.*, 2015, **21**, 1–9.
68 Y. Ge, G. Cheng, N. Xu, W. Wang and H. Ke, *Catal. Sci. Technol.*, 2019, **9**, 4255–4261.
69 J. Sirijaraensre, P. Khongpracha and J. Limtrakul, *Appl. Surf. Sci.*, 2019, **470**, 755–763.
70 M. D. Kumar, S. Sunny and M. Jaccob, *J. CO2 Util.*, 2022, **57**, 101872.
71 Y. Hu, Z. Wei, A. Frey, C. Kubis, C. Y. Ren, A. Spannenberg, H. Jiao and T. Werner, *ChemSusChem*, 2021, **14**, 363–372.
72 S. Kozuch and S. Shaik, *Acc. Chem. Res.*, 2011, **44**(2), 101–110.